Cell Reports
Physical Science

CellPress
OPEN ACCESS

Article

Methylammonium-formamidinium reactivity in aged organometal halide perovskite inks

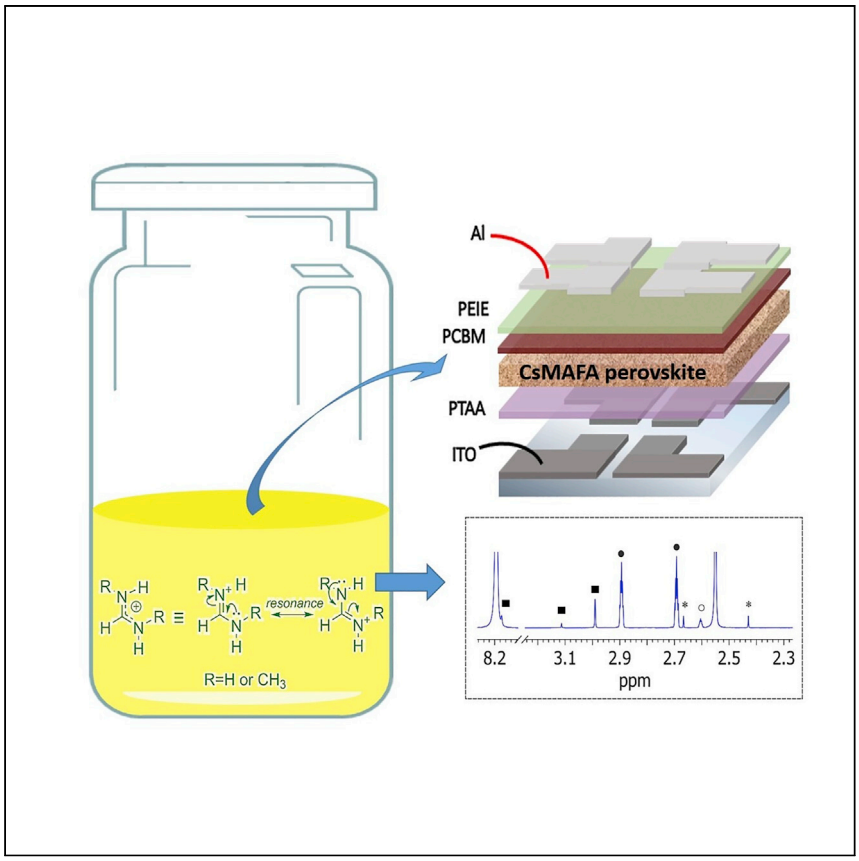

Halide perovskite inks are unstable over time, which negatively effects photovoltaic device performance. This is due to a reaction between the species in solution, studied here using NMR by Valenzano et al., and the kinetics of this can be tuned by adjusting the components/experimental conditions.

Vitantonio Valenzano, Andrea Cesari, Federica Balzano, ..., Aurora Rizzo, Gloria Uccello-Barretta, Silvia Colella

federica.balzano@unipi.it (F.B.)
aurora.rizzo@nanotec.cnr.it (A.R.)
silvia.colella@nanotec.cnr.it (S.C.)

Highlights

Insight into the reactivity of perovskite inks under different experimental conditions

Addition of methylamine to formamidinium gives *trans*/*cis* *N*-methylformamidinium

Cs^+ significantly stabilizes the precursor solution by slowing down the reaction

NMR is a powerful tool to predict solution modifications prior to device fabrication

Valenzano et al., Cell Reports Physical Science *2*, 100432
May 19, 2021 © 2021 The Author(s).
https://doi.org/10.1016/j.xcrp.2021.100432

Cell Reports
Physical Science

CellPress
OPEN ACCESS

Article

Methylammonium-formamidinium reactivity in aged organometal halide perovskite inks

Vitantonio Valenzano,[1,2,6] Andrea Cesari,[3,6] Federica Balzano,[3,*] Antonella Milella,[4,5] Francesco Fracassi,[4,5] Andrea Listorti,[1,4] Giuseppe Gigli,[1,2] Aurora Rizzo,[1,*] Gloria Uccello-Barretta,[3] and Silvia Colella[5,7,*]

SUMMARY

Over the past 10 years, organometal halide perovskites have revolutionized the field of optoelectronics, particularly of emerging photovoltaic technologies. Today's best perovskite solar cells use triple-cation compositions containing a mixture of formamidinium, methylammonium, and cesium to enable more reproducible and stable device performance. The common procedure uses as-prepared precursor ink to avoid an undesirable decrease in device performance, attributed recently to a chemical reaction between methylammonium and formamidinium in solution. Here we employ nuclear magnetic resonance spectroscopy to explore different experimental conditions that can significantly modify these reaction kinetics; in particular, we find that the presence of cesium as the third cation can substantially slow down methylammonium-formamidinium reactivity. Our findings allow us to draw up a protocol for extended overtime perovskite ink stabilization.

INTRODUCTION

The effect of organometal halide perovskites, over the last decade, on optoelectronics and particularly on emerging photovoltaic technologies is extraordinary. They are a class of materials characterized by superior properties combined with mild synthetic protocols. Among many, exceptional characteristics of hybrid halide perovskites, which cannot be found in conventional solution-processed semiconductors, are the long carrier diffusion length (~1 μm)[1] and carrier lifetimes,[1,2] enabling a transport length larger than the depth of absorbed photons and high photovoltaic performance. Mainly used in solar cells[3–5] and light-emitting diodes,[3,6,7] perovskites are formed from solution by self-assembly of precursors. Today's best-performing perovskite solar cells (PSCs) use a mixture of formamidinium (FA), methylammonium (MA), and cesium (Cs) as monovalent cation.[8,9] The resulting triple-cation perovskite compositions enable more reproducible and stable device performance over time[8] compared with FA/MA perovskites, are thermally more robust,[10] contain fewer phase impurities, and are less sensitive to processing conditions. These properties are key for industrialization of perovskite photovoltaics (PV). In particular, the smaller Cs^+ cation (1.81 Å) is added in small amounts to influence the crystal structure by obtaining a decreased effective tolerance factor, which leads to a cubic or pseudo-cubic perovskite structure. Hence, the desired photo-active phase is obtained at room temperature because of entropic stabilization.[10] Saliba et al.[8] developed the first solar cell based on a triple-cation perovskite with mixed halides ($Cs_x(MA_{0.17}FA_{0.83})_{(1-x)}Pb(I_{0.83}Br_{0.17})_3$). Cs^+ can effectively suppress the yellow phase impurities of $FAPbI_3$, providing enhanced and defect-free perovskite

[1]CNR NANOTEC – Istituto di Nanotecnologia, c/o Campus Ecotekne, Via Monteroni, 73100 Lecce, Italy

[2]Dipartimento di Matematica e Fisica "E. De Giorgi," Università del Salento, Campus Ecotekne, Via Arnesano, 73100 Lecce, Italy

[3]Dipartimento di Chimica e Chimica Industriale, Università di Pisa, Via Moruzzi 13, Pisa, PI 56124, Italy

[4]Dipartimento di Chimica, Università degli Studi di Bari Aldo Moro, Via Orabona 4, 70126 Bari, Italy

[5]CNR NANOTEC – Istituto di Nanotechnologia, Dipartimento di Chimica, Università degli Studi di Bari Aldo Moro, Via Orabona 4, 70126 Bari, Italy

[6]These authors contributed equally

[7]Lead contact

*Correspondence:
federica.balzano@unipi.it (F.B.),
aurora.rizzo@nanotec.cnr.it (A.R.),
silvia.colella@nanotec.cnr.it (S.C.)

https://doi.org/10.1016/j.xcrp.2021.100432

This is an open access article under the CC BY-NC-ND license (http://creativecommons.org/licenses/by-nc-nd/4.0/).

thin films, leading to stabilized power conversion efficiency (PCE; up to 1,000 h) exceeding 21%. To date, the best performing triple-cation mixed-halide PSCs have reached a stabilized certified power output of 22.3% for inverted[11] and 25.2% for direct solar cells.[12]

Solution processes are used widely to prepare perovskite absorbers for high-performance solar cells. However, it is commonly accepted among the scientific community that the complex precursor solution needs to be used quickly after preparation to avoid an undesirable decrease in device performance.[8] In light of this, over the last few years, attention has been focused on understanding the chemistry of perovskite precursor solutions. Formation of solution-based intermediates,[13] modification of precursor solutions using additive engineering,[14,15] and Lewis acid-base adduct approaches,[16] have been shown to influence crystallization processes and play an important role in reproducing highly efficient devices comprising the resulting hybrid organic-inorganic active layers. Additionally, Tsai et al.[17] have demonstrated that the optoelectronic properties, crystal size, and device performance of $MAPb(I_{1-x}Cl_x)_3$ are affected by perovskite precursor solution aging. Their optimized aging duration is 48 h, and this leads to an average efficiency of 15.22%.[17] Boonmongkolras et al.[18] also revealed that precursor solution aging has a great influence on colloidal size distribution of the solution, which then affects the phase purity of the films and, eventually, device performance.[18] Their work, using dynamic light scattering (DLS) measurements, revealed formation of micron-sized colloidal intermediates in the triple-cation precursor solution when aged for longer than the optimum time (6 h), which leads to degradation of the phase purity of the resulting films and, consequently, poorer device performance.

Very recently,[19] the decrease in device performance has been attributed to a reaction between MA and FA leading to formation of the new species *N*-methylformamidinium (MFA). Wang et al.[19] used nuclear magnetic resonance (NMR) spectroscopy to identify this species and its formation within 24 h. NMR spectroscopy has been shown to be a key tool to investigate the solution chemistry of perovskite precursors.[20,21] Here we exploited the powerful potential of this technique to study this newly discovered reaction, exploring different experimental conditions that deeply modify the reaction kinetics. We highlight the exceptional role of Cs^+ in stabilization of precursor solution, inhibiting formation of the new species. This adds new insight into triple-cation perovskite chemistry, known to be stabilized in its cubic "black" crystalline phase by addition of Cs^+; our findings demonstrate how the stabilization role of Cs is also extended to the solution. We fabricated PSCs with an inverted layout from precursor solutions at different aging times. The decrease in device performance parallels formation of the new species in solution, allowing us to draw up a guideline for stabilization over time of the precursor solution with the aim of optimizing fabrication of high-performance PSCs.

RESULTS AND DISCUSSION

Perovskite thin films and devices

In this work, the triple cation perovskite $Cs_{0.05}(FA_{0.83}MA_{0.17})_{0.95}Pb(I_{0.83}Br_{0.17})_3$ (CsFAMA), embedding mixed cations and mixed halides, was selected to fabricate state-of-the-art photovoltaic devices in inverted architecture (indium tin oxide [ITO]/poly(triaryl amine) [PTAA]/CsFAMA/[6,6]-phenyl-C61 butyric acid methyl ester [PCBM]/polyethylenimine ethoxylated [PEIE]/aluminum [Al]).[8,22]

As shown in Figure 1A, the inverted p-i-n planar heterojunction device was designed as patterned ITO onto glass substrate/PTAA/PCBM/ PEIE/Al. PTAA was chosen as

CellPress
OPEN ACCESS

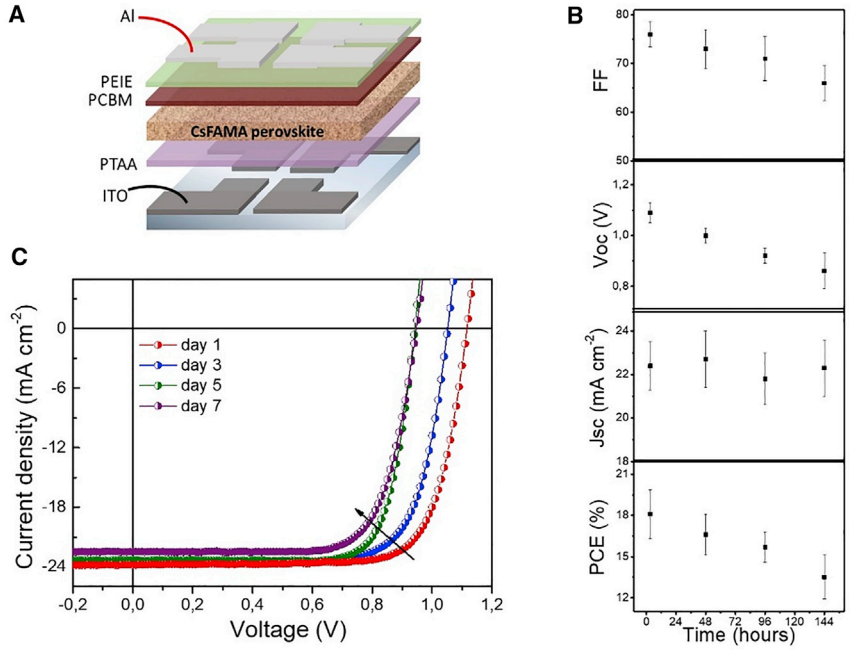

Figure 1. Device fabrication and I-V characteristics over time

(A) Sketch of the PSC device.

(B) Statistic distribution of PV parameters, represented in the graphs as mean calculated on 25 devices error bars represent standard deviation.

(C) J-V curves of the best-performing devices.

the hole-transporting layer (HTL) because of its efficient carrier transport and its high non-wetting properties, which can enhance the overall efficiency of the final device because of the high-aspect-ratio crystalline grain growth.[23] PEIE as the interlayer was found to enhance the device lifetime[24] because of its polymeric nature compared with the standard bathocuproine (BCP). In addition, PEIE has been reported to be an efficient interfacial layer to decrease the work function of the cathode.[25] PSCs were fabricated using freshly prepared precursor solution at different aging times to determine the effect of solution aging on solar cell performance.

For each aging time, 25 devices were fabricated, and their photovoltaic parameters were measured. Figure 1B shows the evolution over time of the PCE, short circuit current density (J_{SC}), open circuit voltage (V_{OC}), and fill factor (FF). Figure 1C shows the typical J-V characteristics of the best-performing CsFAMA devices fabricated at different solution aging times. When examining the results, shown in the Table 1, we saw a systematic decrease of device performance over time. In particular, we obtained the best efficiency with device fabricated within 24 h of preparation of fresh precursor solution. In line with what has been observed previously by Boonmongkolras et al.,[18] the solution needs a few hours to reach complete dissolution of precursors to achieve optimal device performance. The best device showed a state-of-the-art PCE of over 20% with a J_{SC} of 23.8 mA cm^{-2}, an V_{OC} of 1.12 V and an FF of 75.5%.

The PCE decreased from the record 20.1% when employing fresh solution to 18.2% when the solution was 3 days old, 17.2% for 5 days of aging, and 15.6% after 7 days. To characterize the thin film and determine a possible correlation of the structural/optical properties with the changes in performances, we carried out X-ray diffraction (XRD) measurements and photoluminescence characterization at different aging

Table 1. Summary of the average and best device performance at different solution aging times

	FF (%)	V_{OC} (V)	J_{SC} (mA cm^{-2})	PCE (%)
Day 1	76.0 ± 2.6	1.09 ± 0.04	22.4 ± 1.1	18.1 ± 1.8
Best device	75.5	1.12	23.8	20.1
Day 3	73.0 ± 4.0	1.00 ± 0.03	22.7 ± 1.3	16.6 ± 1.5
Best device	73.7	1.05	23.5	18.2
Day 5	71.0 ± 4.5	0.92 ± 0.03	21.8 ± 1.2	15.7 ± 1.1
Best device	77.0	0.96	22.0	17.2
Day 7	66.8 ± 3.7	0.86 ± 0.07	22.3 ± 1.3	13.5 ± 1.6
Best device	73.0	0.95	22.5	15.6

times, and the results are shown in Figure S1 and Figure 2, respectively. The XRD spectra of the as-cast films at different aging times (Figure S1) exhibit peaks that match the black, tetragonal, triple-cation perovskite, corresponding to the well-known composition CsFAMA[8,21] at ~14° (110), ~28° (220) and ~31° (310).[26] The unmodified position of the main peaks indicates that there are no differences in the lattice constant, suggesting that the fraction of halides and cations incorporated in the crystal structure remains the same, as corroborated by X-ray photoelectron spectroscopy (XPS), showing no sign of any significant stoichiometry variation with aging (Table S1). Films deposited from aged solutions present some peculiar features (Figure S1): (1) a decrease in perovskite peak relative intensities and in particular of the (110) reflection, indicating worse crystallinity of the resulting films,[17,18] and (2) appearance of a small side peak at ~11.5° that could be ascribed, in agreement with what has been observed somewhere else, to formation of an undesired perovskite phase including *N*-methylformamidinium, synthesized and characterized previously.[19] The steady-state and time-resolved (TR) photoluminescence (PL) spectra in Figures 2A and 2B also corroborate this possibility. These spectra show, for the freshly measured sample, the typical, relatively broad band of the mixed halide cation perovskite characterized by high intensity and very long radiative lifetime, signs of optimal optoelectronic properties for the material, in line with the superior performance and the device embedding it.

This intense emission is affected by precursor solution aging, in fact both the emission intensity (Figure 2A) that its decay (Figure 2B) decreases with time, and in particular the day 7 solution leads to film with severely reduced emission properties in comparison with the fresh solution, as possible consequence of reduced crystallinity. Besides the reduction in intensity, a slight blue-shift in the PL peak can also be

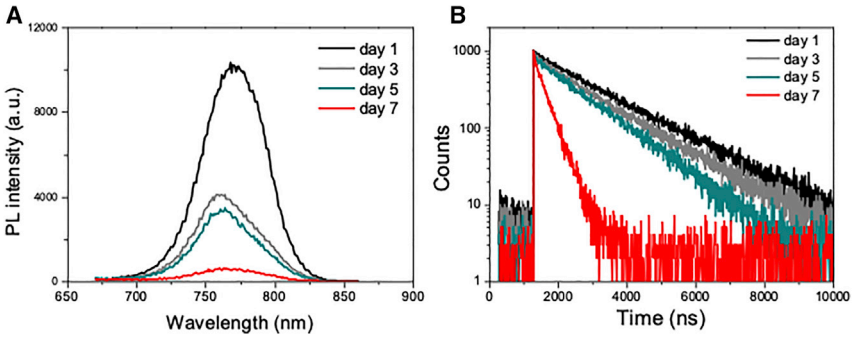

Figure 2. PL data

(A) PL spectra of the CsFAMA mixed perovskite.

(B) Time-resolved PL decay curves over 7 days.

Table 2. Percentage of non-degraded MABr in MABr (0.2 M)/FAI (1 M) in anhydrous solvents and non-anhydrous solvents as detected in ^{1}H NMR spectra (600 MHz, 25°C, DMF/DMSO 9:1).

	MABr (%)	
Time (h)	Anhydrous solvents	Non-anhydrous solvents
0.2	100	100
4	99.5	98.8
15	97.8	95.3

observed, in line with what has been observed previously in a system similar to ours.[19] The presence of the undesired perovskite phase including MFA, detected in our XRD spectra as well as in a previous work,[19] could be the cause of this shift and of the emission intensity decrease.

NMR analysis of precursor solutions

To investigate the reasons for this behavior, we conducted a series of NMR experiments. Each solution prepared for the NMR analysis was obtained by dissolving an appropriate amount of the selected precursors (MA bromide [MABr], FA iodide [FAI], cesium iodide [CsI], PbI_2, and $PbBr_2$), according to the defined stoichiometry. When PbX_2 was used, 2 h of mixing were required for correct solubilization of this salt (vortex, 750 rpm).

First we investigated fresh and aged MABr (0.2 M)/FAI (1 M) solutions in *N*,*N*′-dimethylformamide (DMF)/dimethylsulfoxide (DMSO) 9:1, at the same concentrations employed for photovoltaic device fabrication. Immediately after preparation of the binary mixture (Table 2), only the signals at 2.55 ppm and 8.19 ppm (because of the methyl group of MABr and methine proton of FAI, respectively) together with the broad signal at ~9.00 ppm arising from ammonium were detected in the ^{1}H NMR spectrum (Figure 3A). Interestingly, slight decreases of signal-integrated areas were detected over time, concomitant with the appearance of new resonances at 2.99 ppm, 3.11 ppm, and 8.17 ppm (marked with back squares in Figure 3B), whose percentages were less than 1% after 4 h and about 2% after 15 h. The presence of water traces accelerated formation of degradation products because a roughly 2-fold increase in their amounts was measured after 4 h and 15 h (Table 2).

The beneficial effect of CsI was shown in the mixture MABr/FAI/CsI (0.2:1:0.075) under the experimental conditions employed for device fabrication (25°C, DMF/DMSO 9:1 anhydrous solvents), where more than halved degradation with respect to the mixture MABr/FAI was detected on the basis of the decrease of the ^{1}H NMR signal of MABr (Table 3).

The integrity of precursors was even more preserved (Table 3) in the complete mixture MABr/FAI/CsI/$PbBr_2$/PbI_2, paying great attention to PbI_2 purity. Use of PbI_2 99%, likely contaminated with basic impurities of PbO, produced a dramatic effect, leading to almost complete degradation of the precursors just after 2 h (Table 3). Under these conditions of more accelerated degradation, additional low-intensity signals at 3.22 ppm, 3.10 ppm, and 8.08 ppm were detected in the ^{1}H NMR spectrum (marked with □ in Figure S2).

Accordingly, the MABr/FAI/CsI mixture in the presence of 1.2 mg of PbO (0.008 equivalents, comparable with the amounts of impurities in PbI_2 99%) led to rapid precursor degradation in favor of an appearance of all species observed previously

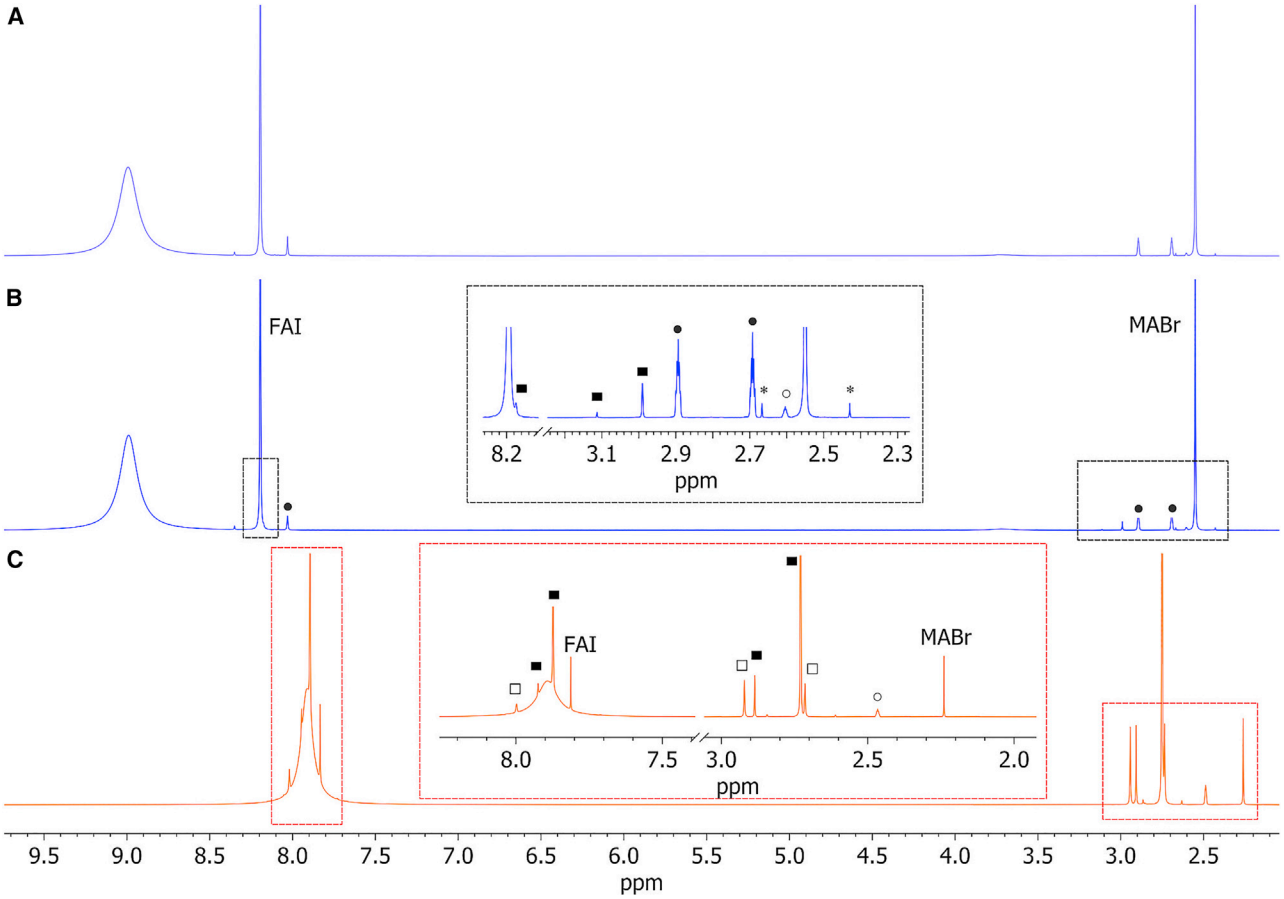

Figure 3. ^{1}H NMR spectra (600 MHz, 25°C)

(A) MABr/FAI 0.2:1 mixture (DMF/DMSO 9:1) immediately after preparation.

(B) MABr/FAI 0.2:1 mixture (DMF/DMSO 9:1) after 15 h.

(C) MABr/FAI 1:1 with 1.2 mg (0.008 equivalents) of PbO (DMSO) after 24 h. Filled squares and empty squares represent for MFA and DMFA species, respectively (*vide infra*). Filled circles and empty circles represent for DMF and DMSO, respectively.

Asterisks represent carbon satellites of MABr.

(Figure S3). Accelerated degradation in a short time (2 h) was also found after addition of a minimum amount of deuterated sodium hydroxide (NaOD) (1% with respect to MABr) to the MABr/FAI 0.2:1 mixture (Figure S4).

To characterize degradation products, we carried out an accurate NMR investigation focused on the nature of the species responsible for the minor signals. The sample

Table 3. Percentage of non-degraded MABr in different precursor mixtures using anhydrous solvents as detected in ^{1}H NMR spectra (600 MHz, 25°C, DMF/DMSO 9:1).

	MABr (%)		
	2 h	4 h	15 h
MABr/FAI (0.2:1)	99.7	99.5	97.8
MABr/FAI/CsI (0.2:1:0.075)	99.9	99.9	99.3
MABr/FAI/CsI/$PbBr_2$/PbI_2 (99.999%) (0.2:1:0.065:0.2:1.1)	99.9	99.9	99.5
MABr/FAI/CsI/$PbBr_2$/PbI_2 (99%) (0.2:1:0.065:0.2:1.1)	0		

that showed the most extensive MABr degradation, MABr/FAI/PbO 1:1:0.008, was selected (Figure 3A). Moreover, after checking that the nature of degradation products was the same in pure DMSO and DMF/DMSO 9:1, we chose to employ pure DMSO to avoid spectral interference because of the residual signals of DMF at 2.89 ppm, 2.69 ppm, and 8.03 ppm (marked as ● in Figure 3B). Only low-frequency shifts of the resonance were observed in DMSO (compared with the DMF/DMSO 9:1 mixture) for the precursors (2.25 ppm, CH_3 of MABr; 7.83 ppm, CH of FAI) and the decomposition products (Figures 3B and 3C).

Regarding the major species marked by filled squares in Figure 3C, heteronuclear single quantum coherence (HSQC) (Figure S5) analysis correlated the two methyl carbons at 28.5 ppm and 33.0 ppm (for the ^{13}C NMR spectrum, see Figure S6) to their respective proton resonances at 2.75 ppm and 2.91 ppm and the two methine carbons at 154.8 ppm and 157.7 ppm to the proton resonances at 7.89 ppm and 7.95 ppm, respectively. Homonuclear scalar correlations (1D total correlation spectroscopy [TOCSY] and 2D correlation spectroscopy (COSY) map; Figures S7 and S8), and long-range heteronuclear correlations (heteronuclear multiple bond correlation [HMBC]; Figure S9) were detected between methine carbons and methyl protons, confirming the existence of two species with equal skeletons and similar chemical environments. A ^{13}C NMR spectrum recorded under quantitative conditions (Figure S6) demonstrated that one single methyl group for each methine was present in their skeleton. Interestingly, slow exchange processes involving the two species were detected in the 1D nuclear Overhauser effect spectroscopy (NOESY) experiments (Figure S10B) and, accordingly, their populations were sensitive to temperature changes (Figure S11). Therefore, the spectroscopic data unequivocally demonstrated the presence of *trans*/*cis* stereoisomeric species produced by the nucleophilic addition of methylamine to FA followed by NH_3 elimination (*trans*-*N*-methylformamidinium [*trans*-MFA] and *cis*-*N*-methylformamidinium [*cis*-MFA]; Scheme 1). As additional proof supporting the suggested mechanism, formation of a basic gaseous species was highlighted through a universal indicator paper positioned on top of the NMR tube. This species was attributed to NH_3 developed during the nucleophilic addition reaction.

The species originating the remaining signals at 2.74 ppm, 2.94 ppm, and 8.02 ppm (marked with □ in Figure 3C) were attributed to the products of further nucleophilic addition of methylamine to methine carbon of MFA, leading to formation of *N*,*N*′-dimethylformamidinium (DMFA; Scheme 1). Two kinds of methyl resonances were detected in the ^1H NMR spectra, corresponding to slow-exchanging stereoisomeric species (1D NOESY; Figure S10C).

The presence in the skeleton of one methine carbon and two methyl groups has been demonstrated unequivocally by quantitative ^{13}C NMR for the dimethylated species (Figure S6). In a recent paper[19] dealing with use of MA iodide (MAI)/FAI/PbI_2-based devices, where the same degradation products were detected in solution by NMR at almost equal chemical shifts, the stereoisomeric nature of MFA and DMFA degradation products was not recognized.[19] To strengthen the correlation between formation of degradation products in solution and a decrease in device performance, we carried out NMR characterization of the complete mixture MABr/FAI/CsI/$PbBr_2$/PbI_2, evaluating the aging effect up to 30 days, as reported in Table S2. The percentage of non-degraded MABr goes from more than 99% for day 1 to ~92% for day 7, demonstrating that devices are sensitive to degradation when it is on the order of a few percentage point, but it is not possible to appreciate smaller differences because of other parameters affecting device performance that could possibly cover this effect.

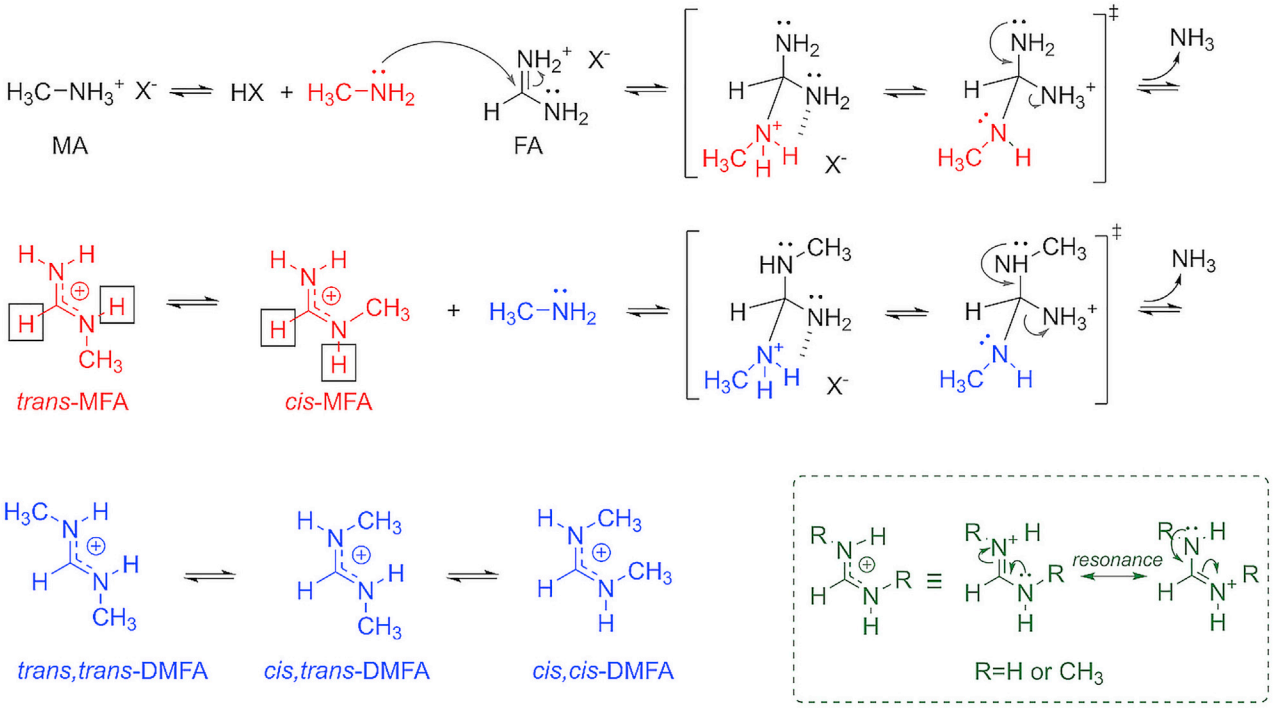

Scheme 1. Proposed mechanism for formation of decomposition products

Shown is the proposed mechanism for formation of decomposition products (MFA and DMFA) in perovskite precursor solution.

The NMR results allowed us to identify crucial parameters influencing the kinetics of the MA/FA reaction; the presence of water and basic impurities dramatically speeds up degradation, whereas addition of CsI seems to stabilize the perovskite precursor mixture for longer, benefitting whole-device efficiency/stability. This result adds a very important piece of knowledge to the chemistry of Cs^+ as a cation in perovskite materials; it seems that its stabilizing effect is not limited to the crystalline structure but that it also extends to the solution. The beneficial effects of Cs^+ on MA/FA perovskite composition are well established, such as enhancing stability under thermal stress and moisture and improving structural stability, as explained by Yi et al.,[10] who showed that Cs is effective in assisting with crystallization of the black phase in FA perovskites because of entropic stabilization. Here we reveal its stabilizing effect on the solution and hypothesize that Cs^+ coordinates part of the methylamine, subtracting it from the formation equilibrium of the new species MFA and DMFA, as depicted in Scheme 1.

A Cs ion can behave as a Lewis acid, coordinating the primary amine via a soft acid-soft base interaction, in a polar aprotic solvent such as DMF or DMSO, where the Cs ion is weakly coordinated by the iodide ion; therefore, such a proximal effect on the amine seems reasonable.[27] This would slow down degradation of MABr.

Through deep NMR characterization, we observe formation of the MFA species as result of the reaction between FA and MA in aged solutions and detect, for the first time, its stereoisomeric nature.

Formation over time, in the solution phase, of these by-products strongly affects final device performance because of modification of the perovskite phase quality after its deposition/formation. These species subtract a certain amount of MA and FA

precursors to the right and well-defined stoichiometric ratio existing for them at the starting point.

We analyze a series of experimental conditions that can affect the reaction kinetics, collecting important information regarding the stabilization of mixed cation perovskite inks.

- The presence of minimum traces of water in solution accelerates (about 2-fold) formation of degradation products, underlining the need for anhydrous conditions during the fabrication process.
- Addition of CsI to the mixture has a beneficial effect on degradation because more than halved degradation product was detected with respect to the MA/FA mixture.
- The presence of small amounts of basic impurities (such as PbO) in the PbI_2 reactant catalyzes the degradation reaction, leading to almost complete degradation of the precursors just after 2 h.

The findings of our investigation provide general guidelines for stabilizing hybrid halide perovskite inks, aiming to improve conditions for industrial-scale manufacturing. In particular, we demonstrate how the presence of Lewis acid species, such as Cs cation, in the ink can stabilize the whole system for aging and *in situ* reactivity, opening a path for a series of investigations of the perovskite solution stability, including a plethora of additives developed and studied so far. We demonstrate how NMR spectroscopy can be a predictive tool for the very first steps of material synthesis; for example, investigating the modifications occurring in solution between perovskite precursors could avoid wasting resources in empirical evaluation of the final devices.

EXPERIMENTAL PROCEDURES

Resource availability

Lead contact

Request for information can be directed to the lead contact, Dr. Silvia Colella (silvia.colella@nanotec.cnr.it).

Materials availability

This study did not generate new material structures.

Data and code availability

This study did not produce new code. All data associated with the work can be found in the article or supplemental information and are available from the authors upon reasonable request.

Materials

All reagents were used without further purification. Lead (II) iodide PbI_2 ultradry 99.999% (metals basis) was purchased from Alfa Aesar. FAI ($\geq$98%, powder), lead (II) bromide ($PbBr_2$; 99.999%, powder) and lead (II) oxide (PbO; 99.999%, trace metals basis) were purchased from Sigma-Aldrich. MABr (>99.5%, recrystallized 4 times) was purchased from Luminescence Technology (Lumtec). CsI (99.999%) was purchased from Sigma-Aldrich.

The solvents, including DMF (99.8%), anhydrous DMSO (99.9%), anhydrous chlorobenzene (CB; 99.8%), toluene, and 2-propanol (isopropanol, IPA) were purchased from Sigma-Aldrich. NaOD (30%) and deuterated solvents (DMSO 99.8% and DMF 99.5%) were purchased from Deutero (Kastellaun, Germany). Commercial anhydrous deuterated solvents were sealed in glass vials.

PTAA was supplied by Aldrich and used as hole transport material. PCBM was purchased from Nano-c and used as electron transport material. PEIE 80% ethoxylated solution 37 wt. in H_2O was purchased from Aldrich and used as a hole-blocking layer.

Perovskite precursor solution

The CsFAMA mixed-perovskite precursor solutions were deposited from a modified Saliba's recipe[8] in which the components FAI (1 M), PbI_2 (1.1 M), MABr (0.2 M), $PbBr_2$ (0.2 M), and CsI (0.065 M) were dispersed in a mixture of DMF:DMSO = 9:1 (v:v). The choice of this solvent ratio as a medium for dispersing all perovskite precursors was based on a standard Park recipe. The CsFAMA solution was stirred vigorously at room temperature for several hours before use.

Photovoltaic device fabrication and characterization

ITO-coated glass substrates, 4L patterned, were cleaned by ultrasonication in deionized water, acetone, and then 2-propanol. The perovskite precursor solution was deposited by a consecutive two-step spin-coating process at 1,000 and 6,000 rpm for 10 and 20 s, respectively, onto a PTAA layer (starting from 1.5 mg/mL toluene solution) using CB as anti-solvent. The process was carried out under controlled atmospheric conditions with a humidity of less than 1% and a temperature between 20°C and 25°C. After spin coating of the perovskite precursor solution, the substrates were transferred to a hot plate and heated at 100°C ± 5°C for 10 min. Subsequently, the PCBM solution (25 mg/mL CB) was filtered with a 0.20-μm filter and then spin coated at 1,000 rpm for 60 s. Then an ultrathin layer of PEIE was spin coated on top of PCBM. Finally, an Al metal electrode of about 100 nm was thermally evaporated at a pressure of 4×10^{-6} mbar on top of the HTM layer to form the back contact. The active area of the complete device was 0.04 cm^{-2}. The devices were characterized using a Keithley 2400 Source Measure Unit and AirMass 1.5 Global (AM 1.5G) solar simulator (Newport 91160A) with an irradiation intensity of 100 mW/cm^2. The solar simulator irradiance was set to 100 $mW \cdot cm^{-2}$ using a thermopile radiant power meter with a fused-silica window (Spectra 3 Physics Oriel, model 70260). The active area of the complete device was 0.04 cm^{-2}. All devices were tested using 100 mV/s or 1000 mV/s scan rates under nitrogen at 22°C.

PL

Steady-state and time-resolved PL was measured by an Edinburgh FLS920 spectrometer equipped with a Peltier-cooled Hamamatsu R928 photomultiplier tube (185–850 nm). An Edinburgh Xe900 450-W Xenon arc lamp was used as an excitation light source. The details of the experimental procedures have been described elsewhere.[20]

Corrected spectra were obtained via a calibration curve supplied with the instrument (lamp power in the steady-state PL experiments, 0.6 mW cm^{-2}; spot area, 0.5 cm^2). Emission decay time was determined with the single-photon counting technique by means of the same Edinburgh FLS980 spectrometer using a laser diode as the excitation source (1 MHz, exc = 635 nm, 67-ps pulse width and about 30-ps time resolution after deconvolution) and a Hamamatsu MCP R3809U-50 (time resolution, 20 ps) as a detector (laser power in the TRPL experiment, 1.6 W cm^{-2}; spot area, 0.3 mm^2).

NMR

NMR measurements were performed on an INOVA600 spectrometer (Varian, Palo Alto, CA, USA) operating at 600 MHz for ^1H and 150 MHz for ^{13}C. The spectra are referenced through the solvent lock (^2H) signal according to the IUPAC-recommended secondary referencing method. The temperature was controlled to 25°C ± 0.1°C through a Varian control unit. 2D NMR spectra were obtained by using

standard sequences. The spectral width used was the minimum required in both dimensions. 2D gradient HSQC (gHSQC) was obtained with a 1.2-s relaxation delay and 64 scans for each of the 128 increments. 1D TOCSY spectra were recorded by selecting a specific frequency with a mixing time of 0.15 s, a delay of 1 s, and 512 scans. 2D gradient HMBC (gHMBC) was obtained with a 1.2 s relaxation delay and 64 scans for each of the 128 increments. The quantitative ^{13}C NMR spectrum was recorded using a d_1 of 20 s with an inversely gated decoupling pulse sequence. 1D NOESY spectra were recorded by selecting a specific frequency with a mixing time of 0.8 s, a delay of 1 s, and 256 scans.

XPS

XPS analyses were performed with a scanning XPS microprobe (PHI 5000 Versa Probe II, Physical Electronics) equipped with a monochromatic Al Kα X-ray source (1,486.6 eV) operated at 15 kV and 24.8 W with a spot of 100 μm. Survey (0–1,200 eV) and high-resolution spectra (C1s, O1s, N1s, Cs3d, Br3d, I3d, and Pb4f) were recorded in FAT (fixed analyzer transmission) mode at a pass energy of 117.40 and 29.35 eV, respectively. The analyzer energy resolution, evaluated on the Full Width at Half Maximum (FWHM) Ag 3d5/2 photoemission line, was 0.7 eV for a pass energy of 29.35 eV. Surface charging was compensated using dual-beam charge neutralization with a flux of low-energy electrons (~1 eV) combined with very-low-energy Ar^+ ions (10 eV). The hydrocarbon component of the C1s spectrum was used as an internal standard for charging correction, and it was fixed at 285.0 eV. All spectra were collected at an angle of 45° with respect to the sample surface. Best fit of the high-resolution spectra was carried out with MultiPak (Physical Electronics) data processing software. Atomic concentrations were determined from the high-resolution spectra after subtracting a Shirley-type background, using the Scofield sensitivity factors set in the MultiPak software. For each sample, quantitative data were averaged on five replicates. Source power and analysis time were optimized to avoid sample degradation upon X-ray exposure.

SUPPLEMENTAL INFORMATION

Supplemental information can be found online at https://doi.org/10.1016/j.xcrp.2021.100432.

ACKNOWLEDGMENTS

V.V., A.R., G.G., and S.C. acknowledge PON Project "Tecnologia per celle solari bifacciali ad alta Efficienza a 4 terminali per utility scale" (BEST-4U) of the Italian Ministry MIUR (CUP B88D19000160005).

AUTHOR CONTRIBUTIONS

V.V., A.C., A.R., F.B., A.M., and A.L. conducted the experiments. G.G., F.F., and G.U.B. acquired funding. F.B. and S.C. designed the experiments. S.C. supervised and S.C., A.R., and G.U.B. wrote the paper. All authors discussed the results and commented on the manuscript.

DECLARATION OF INTERESTS

The authors declare no competing interests.

Received: December 27, 2020
Revised: March 26, 2021
Accepted: April 21, 2021
Published: May 19, 2021

REFERENCES

1. Chen, Z., Turedi, B., Alsalloum, A.Y., Yang, C., Zheng, X., Gereige, I., Alsaggaf, A., Mohammed, O.F., and Bakr, O.M. (2019). Single-Crystal MAPbI3 Perovskite Solar Cells Exceeding 21% Power Conversion Efficiency. ACS Energy Lett. *4*, 1258–1259.
2. Gong, J., Flatken, M., Abate, A., Correa-Baena, J.P., Mora-Seró, I., Saliba, M., and Zhou, Y. (2019). The Bloom of Perovskite Optoelectronics: Fundamental Science Matters. ACS Energy Lett. *4*, 861–865.
3. Stranks, S.D., and Snaith, H.J. (2015). Metal-halide perovskites for photovoltaic and light-emitting devices. Nat. Nanotechnol. *10*, 391–402.
4. Li, C., Wang, A., Xie, L., Deng, X., Liao, K., Yang, J.A., Li, T., and Hao, F. (2019). Emerging Alkali Metal Ion (Li+, Na+, K+ and Rb+) Doped Perovskite Films for Efficient Solar Cells: Recent Advances and Prospects. J. Mater. Chem. A Mater. Energy Sustain. *7*, 24150–24163.
5. Chen, Y., Zhang, L., Zhang, Y., Gao, H., and Yan, H. (2018). Large-Area Perovskite Solar Cells-a Review of Recent Progress and Issues. RSC Advances *8*, 10489–10508.
6. Giuri, A., Yuan, Z., Miao, Y., Wang, J., Gao, F., Sestu, N., Saba, M., Bongiovanni, G., Colella, S., Esposito Corcione, C., et al. (2018). Ultra-Bright Near-Infrared Perovskite Light-Emitting Diodes with Reduced Efficiency Roll-off. Sci. Rep. *8*, 15496.
7. Colella, S., Mazzeo, M., Rizzo, A., Gigli, G., and Listorti, A. (2016). The Bright Side of Perovskites. J. Phys. Chem. Lett. *7*, 4322–4334.
8. Saliba, M., Matsui, T., Seo, J.Y., Domanski, K., Correa-Baena, J.P., Nazeeruddin, M.K., Zakeeruddin, S.M., Tress, W., Abate, A., Hagfeldt, A., and Grätzel, M. (2016). Cesium-containing triple cation perovskite solar cells: improved stability, reproducibility and high efficiency. Energy Environ. Sci. *9*, 1989–1997.
9. Yang, W.S., Park, B.W., Jung, E.H., Jeon, N.J., Kim, Y.C., Lee, D.U., Shin, S.S., Seo, J., Kim, E.K., Noh, J.H., and Seok, S.I. (2017). Iodide management in formamidinium-lead-halide-based perovskite layers for efficient solar cells. Science *356*, 1376–1379.
10. Yi, C., Luo, J., Meloni, S., Boziki, A., Ashari-Astani, N., Grätzel, C., Zakeeruddin, S.M., Röthlisberger, U., and Grätzel, M. (2016). Entropic Stabilization of Mixed A-Cation ABX3 Metal Halide Perovskites for High Performance Perovskite Solar Cells. Energy Environ. Sci. *9*, 656–662.
11. Zheng, X., Hou, Y., Bao, C., Yin, J., Yuan, F., Huang, Z., Song, K., Liu, J., Troughton, J., Gasparini, N., et al. (2020). Managing Grains and Interfaces via Ligand Anchoring Enables 22.3%-Efficiency Inverted Perovskite Solar Cells. Nat. Energy *5*, 131–140.
12. National Renewable Energy Laboratory (2020). Best Research-Cell Efficiency Chart. https://www.nrel.gov/pv/cell-efficiency.html.
13. Hamill, J.C., Schwartz, J., and Loo, Y.L. (2018). Influence of Solvent Coordination on Hybrid Organic-Inorganic Perovskite Formation. ACS Energy Lett. *3*, 92–97.
14. Han, G., Hadi, H.D., Bruno, A., Kulkarni, S.A., Koh, T.M., Wong, L.H., Soci, C., Mathews, N., Zhang, S., and Mhaisalkar, S.G. (2018). Additive Selection Strategy for High Performance Perovskite Photovoltaics. J. Phys. Chem. C *122*, 13884–13893.
15. Li, T., Pan, Y., Wang, Z., Xia, Y., Chen, Y., and Huang, W. (2017). Additive Engineering for Highly Efficient Organic-Inorganic Halide Perovskite Solar Cells: Recent Advances and Perspectives. J. Mater. Chem. A Mater. Energy Sustain. *5*, 12602–12652.
16. Lee, J.W., Kim, H.S., and Park, N.G. (2016). Lewis Acid-Base Adduct Approach for High Efficiency Perovskite Solar Cells. Acc. Chem. Res. *49*, 311–319.
17. Tsai, H., Nie, W., Lin, Y.H., Blancon, J.C., Tretiak, S., Even, J., Gupta, G., Ajayan, P.M., and Mohite, A.D. (2017). Effect of Precursor Solution Aging on the Crystallinity and Photovoltaic Performance of Perovskite Solar Cells. Adv. Energy Mater. *7*, 1–9.
18. Boonmongkolras, P., Kim, D., Alhabshi, E.M., Gereige, I., and Shin, B. (2018). Understanding Effects of Precursor Solution Aging in Triple Cation Lead Perovskite. RSC Advances *8*, 21551–21557.
19. Wang, X., Fan, Y., Wang, L., Chen, C., Li, Z., Liu, R., Meng, H., Shao, Z., Du, X., Zhang, H., et al. (2020). Perovskite Solution Aging: What Happened and How to Inhibit? Chem *6*, 1369–1378.
20. Masi, S., Aiello, F., Listorti, A., Balzano, F., Altamura, D., Giannini, C., Caliandro, R., Uccello-Barretta, G., Rizzo, A., and Colella, S. (2018). Connecting the solution chemistry of PbI_2 and MAI: a cyclodextrin-based supramolecular approach to the formation of hybrid halide perovskites. Chem. Sci. (Camb.) *9*, 3200–3208.
21. Masi, S., Rizzo, A., Aiello, F., Balzano, F., Uccello-Barretta, G., Listorti, A., Gigli, G., and Colella, S. (2015). Multiscale morphology design of hybrid halide perovskites through a polymeric template. Nanoscale *7*, 18956–18963.
22. Jeon, N.J., Noh, J.H., Yang, W.S., Kim, Y.C., Ryu, S., Seo, J., and Seok, S.I. (2015). Compositional engineering of perovskite materials for high-performance solar cells. Nature *517*, 476–480.
23. Bi, C., Wang, Q., Shao, Y., Yuan, Y., Xiao, Z., and Huang, J. (2015). Non-wetting surface-driven high-aspect-ratio crystalline grain growth for efficient hybrid perovskite solar cells. Nat. Commun. *6*, 7747.
24. Venkatesan, S., Ngo, E., Khatiwada, D., Zhang, C., and Qiao, Q. (2015). Enhanced Lifetime of Polymer Solar Cells by Surface Passivation of Metal Oxide Buffer Layers. ACS Appl. Mater. Interfaces *7*, 16093–16100.
25. Dong, S., Wan, Y., Wang, Y., Yang, Y., Wang, Y., Zhang, X., Cao, H., Qin, W., Yang, L., Yao, C., et al. (2016). Polyethylenimine as a Dual Functional Additive for Electron Transporting Layer in Efficient Solution Processed Planar Heterojunction Perovskite Solar Cells. RSC Advances *6*, 57793–57798.
26. Yu, Y., Yang, S., Lei, L., Cao, Q., Shao, J., Zhang, S., and Liu, Y. (2017). Ultrasmooth Perovskite Film via Mixed Anti-Solvent Strategy with Improved Efficiency. ACS Appl. Mater. Interfaces *9*, 3667–3676.
27. Salvatore, R.N., Nagle, A.S., and Jung, K.W. (2002). Cesium effect: high chemoselectivity in direct N-alkylation of amines. J. Org. Chem. *67*, 674–683.